JOC The Journal of Organic Chemistry

Article

pubs.acs.org/joc

Formation of Aza-*ortho*-quinone Methides Under Room Temperature Conditions: Cs_2CO_3 Effect

Daniel M. Walden,[†] Ashley A. Jaworski,[‡] Ryne C. Johnston,[†] M. Todd Hovey,[‡] Hannah V. Baker,[†] Matthew P. Meyer,[§] Karl A Scheidt,*[,‡] and Paul Ha-Yeon Cheong*[,†]

[†]Department of Chemistry, Oregon State University, 135 Gilbert Hall, Corvallis, Oregon 97331, United States

[‡]Department of Chemistry, Northwestern University, 2145 Sheridan Rd, Evanston, Illinois 60208, United States

[§]Department of Chemistry and Biochemistry, University of California, Merced, California 95453, United States

Supporting Information

ABSTRACT: Since the first report of a facile, room temperature process to access aza-*ortho*-quinone methides (aoQMs) by Corey in 1999, this chemistry has remained dormant until our report of an enantioselective catalytic example in 2014. We report a theoretical and experimental study of the key to success behind these successful examples to enable broader exploitation of this useful intermediate. We have discovered that transformations involving the aoQM are remarkably facile with barriers <17 kcal/mol. The main difficulty of exploiting aoQM in synthesis is that they are unstable (ΔG > 30 kcal/mol), precluding their formation under mild conditions. The use of Cs_2CO_3 as base is critical. It provides a thermodynamically and kinetically favorable means to form aoQMs, independent of the salt solubility and base strength. The exothermic formation of salt byproducts provides a driving force (average ΔG = −30.8 kcal/mol) compensating for the majority of the inherent unfavorable thermodynamics of aoQM formation.

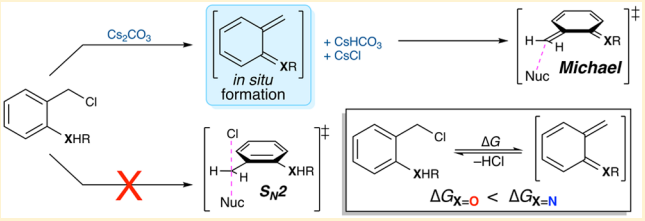

INTRODUCTION

Quinone methides, particularly *ortho*-quinone methides (oQMs), are highly reactive and useful intermediates[1] with numerous examples in synthetic methodologies,[2] total syntheses,[3] and natural product chemistry.[4] A multitude of reports disclose oQM use under mild conditions.[5] In contrast, reports of *in situ* generation of aza-*ortho*-quinone methides (aoQMs) as reactive intermediates under mild conditions are demonstrably rare (Scheme 1, top).[6] E.J. Corey first reported the use of aoQMs as useful reactive intermediates in 1999,[7] and for more than a decade, this chemistry remained underexplored until our report in 2014.[8] While there are examples of aoQMs being formed as a result of pyrolysis, photolysis, with nonremovable stabilizing groups,[9] or from even more reactive precursors,[10] the difficulty of its generation under mild conditions have limited aoQMs as general electrophiles in catalysis and synthesis.

In this report, we studied three reactions that can proceed through aoQM intermediacy using experiments and theory.[11] We have identified the enabling factor behind successful cases of aoQM-mediated reactions under mild conditions. Herein, we describe the thermodynamic and kinetic effect Cs_2CO_3 has in accessing the reactive aoQM intermediate in synthesis and asymmetric catalysis. Our results highlight and refine the cesium effect[12] that has been at the forefront of many organic reactions that take place under basic conditions. While this current study focuses on the use of *ortho* substituted benzyl chloride precursors as substrates, we will continue to leverage our newfound understanding to develop novel substrates for aoQM-mediated reactions.

RESULTS AND DISCUSSION

Computational Details. Geometry optimizations were performed with the M06-2X method[13] with SDD+ECP for Cs and 6-31G(d)[14] basis sets for all other atoms. Solvation was modeled implicitly[15] using PCM[16] with the solvent employed in the experiments. Geometry optimizations, vibrational frequency analysis, and PCM solvation was completed using Gaussian 09.[17] Energy refinements were computed at M06-2X/def2-QZVPP[18] using the ORCA computational package[19] with PCM solvation corrections at M06-2X/6-311++G(2df,p)[20] and SDD+ECP using Gaussian 09.

Reliable energetics involving partially heterogeneous, strongly ionic acid/base reactions in which constituent reactants, intermediates, or products can potentially dimerize/oligomerize are theoretically challenging at present, and these results should be taken as a model process that assumes homogeneity, precluding nucleation/oligomerization and other experimental anomalies. Regardless, the key discovery here is that the Cs_2CO_3 is critical in effecting aoQM formation under mild conditions.

Received: March 24, 2017
Published: June 26, 2017

DOI: 10.1021/acs.joc.7b00697
J. Org. Chem. 2017, 82, 7183−7189

Scheme 1. Summary of oQM Chemistry and Recent aoQM Chemistry

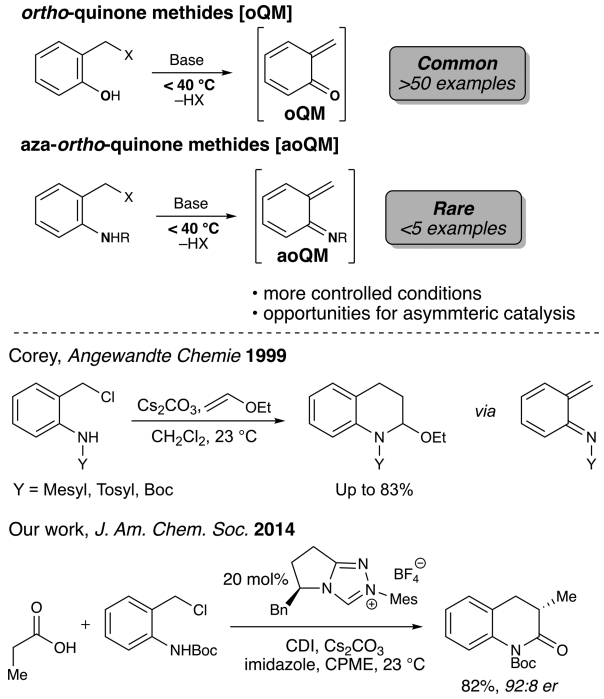

Inherent Stability of aoQM vs oQM. The discrepancy between the proliferation of oQM over aoQM mediated reactions was first investigated. We evaluated the effect of the heteroatom on the quinone equilibria. The computed equilibria in dichloromethane, diethyl ether, and tetrahydrofuran between the *ortho* substituted benzyl chloride precursor and their corresponding methides are shown in Table 1. The oQM is more stable than the aoQM by ~10 kcal/mol, corresponding to ~10^7-fold ease of forming the oQM at room temperature. This may explain the prevalence of the former in literature. The stability differences are attributed to the relative π-bond strengths between carbon and the heteroatoms. The stronger, more polarized C=O π-bond in the oQM derivatives helps mitigate the energetic penalty of losing aromaticity. The C=O π-bond is stronger than C=N π-bond by 10–15 kcal/mol, matching the stability differences between oQM and aoQM.[21]

Table 1. Computed *ortho*-Quinone and Aza-*ortho*-quinone Methide Equilibria

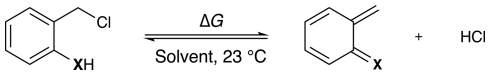

X	ΔG (DCM)	ΔG (DEE)	ΔG (THF)
O	19.6	19.9	19.7
NH	29.1	29.3	29.1
NBoc	32.9	33.4	33.0

Cesium Carbonate Equilibrium Facilitates aoQM Production. Any reaction which generates methides must overcome the resonance energy of benzene.[22] Under harsh conditions, much of this energy will come from light or heat. Under milder reaction conditions, the harnessing of chemical energy will play a much larger role. We postulated that the basic conditions used to generate these reactive intermediates may be responsible in mitigating the unfavorable thermodynamics. Specifically, we considered the thermodynamic effect of converting Cs_2CO_3 and HCl to $CsHCO_3$ and CsCl. Computations showed that this reaction is highly exergonic in three different polar aprotic solvents (ΔG_{avg} = −30.8 kcal/mol, blue arrows, Chart 1). By coupling this reaction with the aoQM formation process, aoQMs were now shown to be in equilibrium with the *ortho* amino benzyl chloride precursors under ambient conditions (ΔG aoQM 1.7–3.2 kcal/mol).

Chart 1. Affect of *in Situ* Salt Formation on aoQM Thermodynamics with Imidazole and Cesium Carbonate as Base

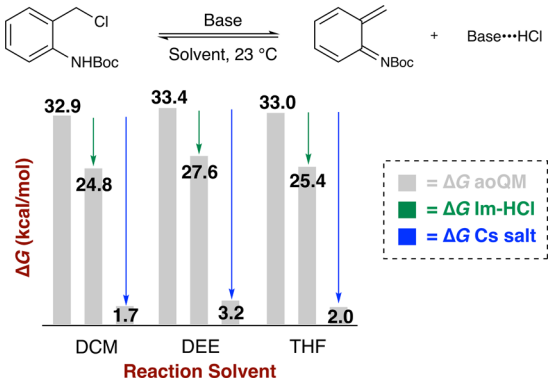

We wondered if other more moderate bases, such as imidazole, behave similarly. Computations suggested that the complexation of an imidazole to the *in situ* generated HCl puts the NBoc-protected aoQM at ~25 kcal/mol (ΔG_{avg} = 25.9 kcal/mol, Chart 1, green arrows). The thermodynamic stabilization afforded by the formation of an imidazole-HCl complex is ~8 kcal/mol, which would predict little aoQM formation at room temperature from thermodynamics alone.[23]

Mechanistic Analysis of aoQM Formation. Three pathways for aoQM formation can be envisioned (Figure 1), beginning with fast deprotonation of the labile amine proton by cesium carbonate (**Deprotonation-TS**, $\Delta G^{\ddagger}$ = 3.6 kcal/mol). All computed mechanisms originate from the postdeprotonation cesium complex (ΔG = 0.4 kcal/mol). Two modes of intramolecular S_N2 attack[24] followed by electrocyclic ring opening were considered (magenta and blue pathways). While the barrier of **6-exotet-TS** ($\Delta G^{\ddagger}$ = 24.6 kcal/mol) lies close to the estimated experimental barrier, the intermediate that follows presents a significant thermodynamic sink (ΔG = −18.1 kcal/mol). The stability of this intermediate hinders **Oxazine-opening-TS** from occurring, even if electrocyclic ring opening gives a reasonable barrier from starting material ($\Delta G^{\ddagger}$ = 21.4 kcal/mol). The computed barrier to **Oxazine-opening-TS** of 39.5 kcal/mol (relative to the benzoxazine intermediate) is consistent with computed and experimental barriers of retro-Diels–Alder reactions of 1,2-benzoxazines to form oQMs.[25] A similar trend is observed for **6-exotet-TS**, although both the initial ring closure ($\Delta G^{\ddagger}$ = 33.7 kcal/mol) and **Azitidine-opening-TS** ($\Delta G^{\ddagger}$ = 38.8 kcal/mol) are highly disfavored regardless of the thermodynamics of the fused ring intermediate. Ultimately, simple elimination of the chloride leaving group is computed as the favored pathway (**Elimination-TS**, $\Delta G^{\ddagger}$ = 12.1 kcal/mol).

Elimination of the chloride leaving group results in loss of aromaticity, typically seen as a formidable hurdle in most room temperature reactions. Complexation of the cesium cation with

DOI: 10.1021/acs.joc.7b00697
J. Org. Chem. 2017, 82, 7183–7189

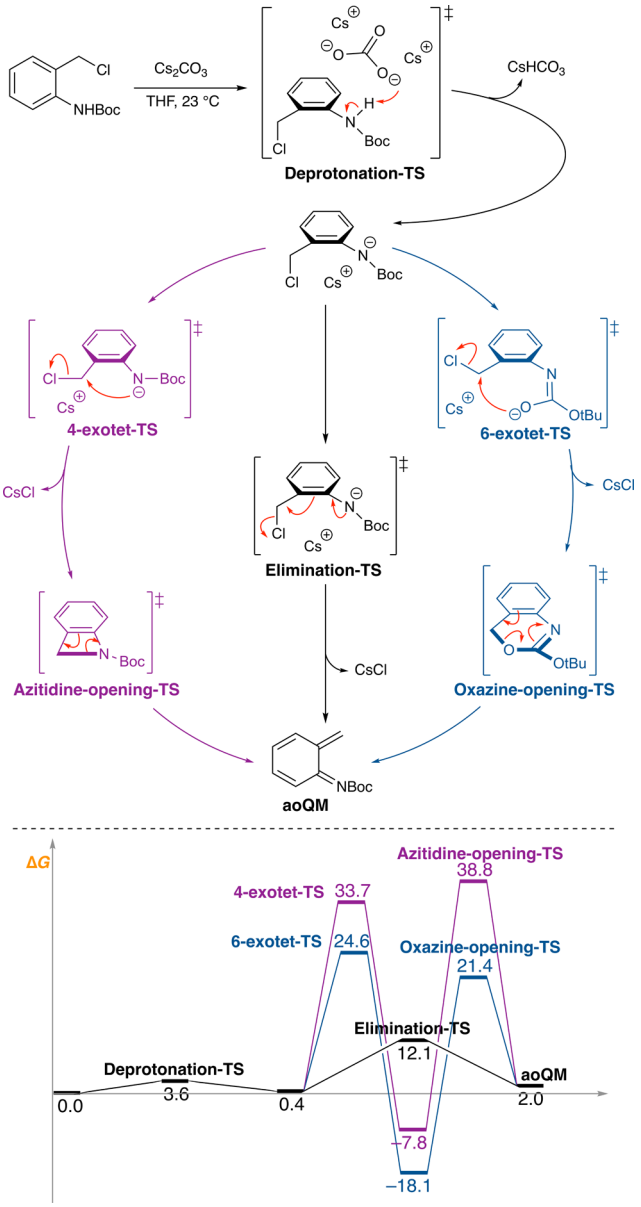

Figure 1. Computed mechanisms of aoQM formation in THF solvent. Stepwise deprotonation followed by chloride elimination is the favored mechanism (black) over intramolecular S_N2 and ring-opening (blue and magenta).

the departing leaving group and the partially anionic nitrogen atom (Figure 2, **Elimination-TS**) is hypothesized to offset this

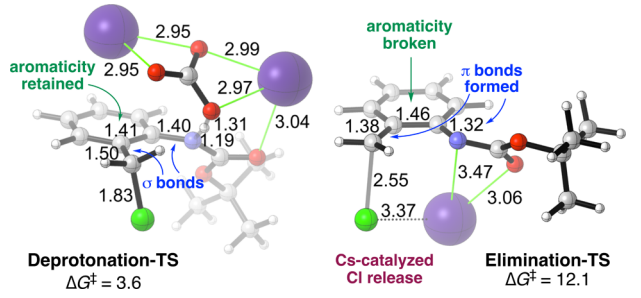

Figure 2. Computed TSs[26] of the stepwise deprotonation/elimination mechanism for aoQM formation.

penalty to the point of facile aoQM formation under ambient conditions. Considering that the equilibrium between the *ortho* substituted benzyl chloride precursor and cesium bicarbonate slightly favors the starting material by 0.4 kcal/mol, it is proposed that the main driving force is the formation of the ionic Cs−Cl bond itself. This effect is apparent is the highly exergonic formation of the fused azitidine (ΔG = −7.8 kcal/mol) and oxazine ring (ΔG = −18.1 kcal/mol) intermediates (Figure 1, bottom), where aromaticity is intact and ring formation is concomitant with CsCl salt formation.

Applications to Dihydroquinolone Synthesis. Corey's dihydroquinolone reaction was hypothesized to occur via a concerted or stepwise Diels−Alder to an aoQM generated *in situ*. From our previous computations, we can already predict that the cesium carbonate in solution will render the aoQM accessible under room temperature conditions. What is unknown is whether an alternative mechanism competes with the subsequent cycloaddition step. One such possible mechanism is direct nucleophilic substitution, in which the vinyl ether may directly add to the aoQM precursor via S_N2-like transition state followed by loss of HCl and cyclization to furnish the observed dihydroquinolone product (**Corey-S_N2-TS**, Figure 3, top panel). The developing negative charge of the departing chloride is stabilized by the vicinal N−H (2.41 Å). Even with the anionic Cl leaving group stabilized through hydrogen bonding, the S_N2 barrier is considerably high (37.3 kcal/mol). The most favorable pathway is formation of the aoQM (ΔG = 2.0 kcal/mol) followed by concerted [4+2] (**Corey-Diels−Alder-TS**, $\Delta G^{\ddagger}$ = 17.8 kcal/mol). In the absence of cesium carbonate, no reaction is expected to occur given the high energy of the S_N2 ($\Delta G^{\ddagger}$ = 37.3 kcal/mol) and [4+2] ($\Delta G^{\ddagger}$ = 48.8 kcal/mol) pathways, both which lie far below the estimated barrier of 24 kcal/mol.

Analysis of the NHC-catalyzed asymmetric dihydroquinolone synthesis reveals similar energetic trends (Figure 3, bottom panel). While the nucleophilic substitution pathway is lower in energy than the Corey example (**S_N2-TS**, $\Delta G\ddagger$ = 29.2 kcal/mol), it still lies above the estimated room temperature barrier, and significantly below the **Major-Michael-TS-(*S*)** ($\Delta G\ddagger$ = 13.5 kcal/mol) as mediated by aoQM formation. Dihydroquinolone formation is stepwise, beginning with Michael addition and followed by cyclization (**Cyclization-TS**, $\Delta G^{\ddagger}$ = −15.2 kcal/mol). Release of the NHC from the resultant tetrahedral intermediate leads to product and begins a new catalytic cycle.

Enantioselectivity as Theoretical Evidence for aoQMs. Unlike the achiral Corey example, stereoselectivity is critical in the NHC-catalyzed reaction. Our goal is to develop a stereocontrol model that assumes an aoQM mediated stereodetermining C−C bond formations step. Agreement of the computed enantioselectivity with experiment provides additional evidence for aoQM intermediacy.

In both the major and minor stereodeterming Michael TSs (Figure 4), the developing negative charge on the nitrogen of the aoQM in the transition state is mitigated by the proximity to the positively charged heterocycle of the NHC catalyst. Conjugative stabilization of the developing negative charge on the nitrogen by the BOC group is not realized in these transition states, the π/π^* system of the BOC group is orthogonal to the conjugated π system of the aoQM (∠C═N/C═O = ~95°) responsible for charge delocalization resulting from nucleophilic attack of the aoQM in the transition state. Moreover, the nitrogen is bent significantly (~120°), indicating

DOI: 10.1021/acs.joc.7b00697
J. Org. Chem. 2017, 82, 7183−7189

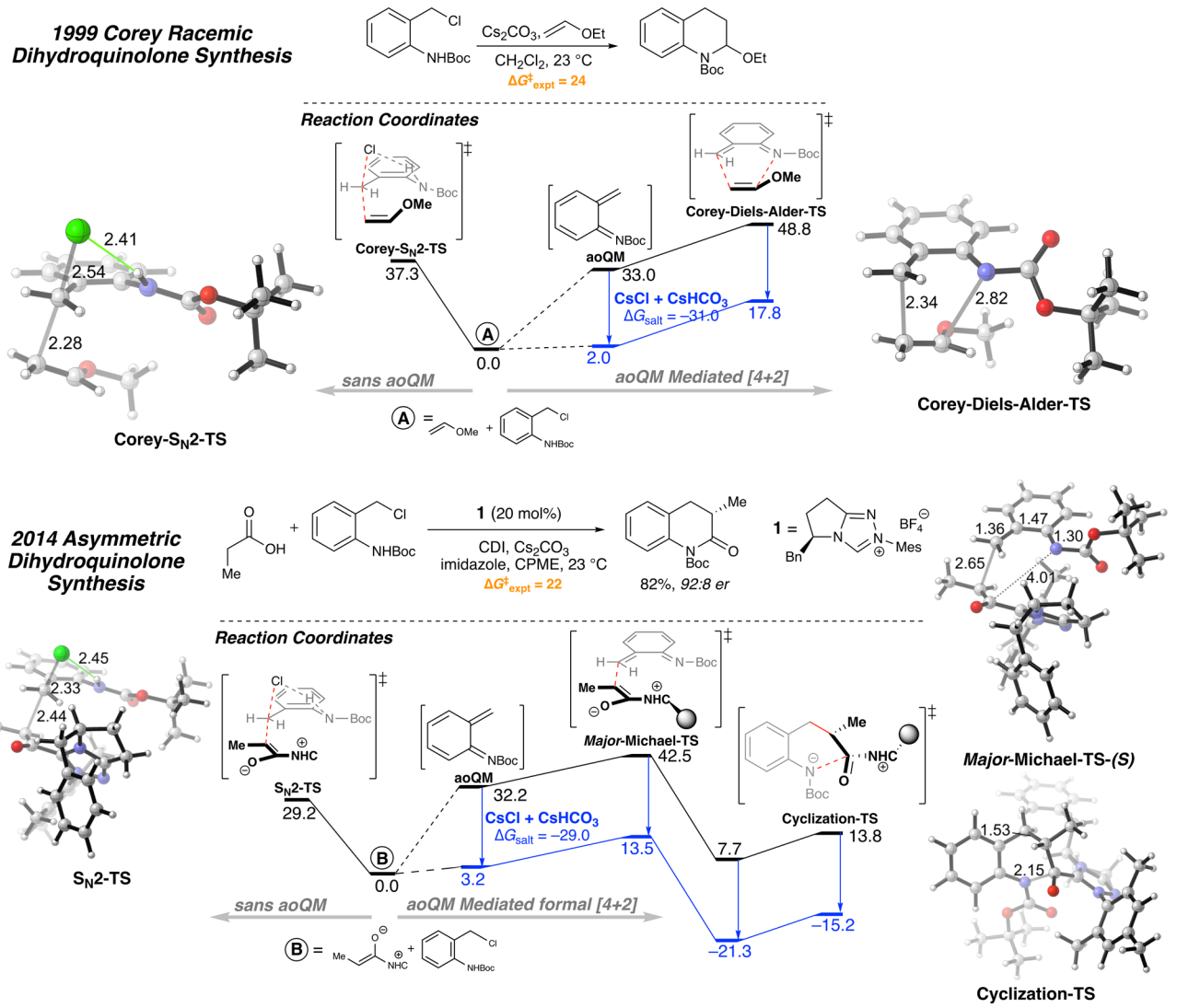

Figure 3. Corey's dihydroquinolone synthesis from vinyl ethers (top); NHC-**1**-catalyzed dihydroquinolone synthesis from propanoic acid (bottom). Bidirectional reaction coordinate diagrams shown. To the right, two energetics for the aoQM-mediated reaction: parent reaction without formation of any salt byproducts (black) and with Cs_2CO_3 salt byproducts (CsCl + $CsHCO_3$, blue). To the left, energetics for the non-aoQM mediated S_N2 process.

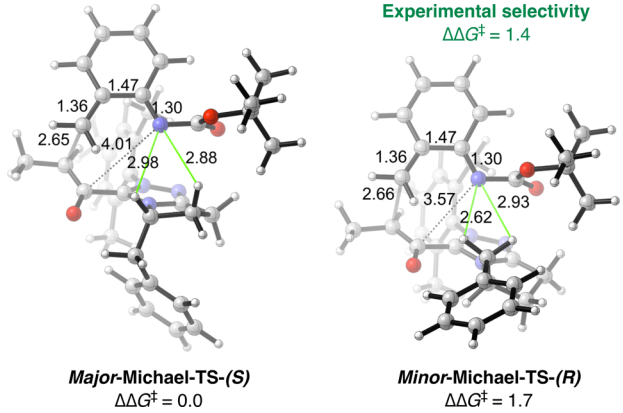

Figure 4. Enantiodetermining transition structures of NHC **1** catalyzed dihydroquinolone synthesis from propanoic acid (Figure 1, bottom panel). Green lines represent stabilizing CH···N interactions.

that charge delocalization of the in-plane lone pair is also not present.

Enantiocontrol arises from differential stabilization of the developing negative charge at the nitrogen of the aoQM in the Michael step. Both transition structures experience proximity of the aoQM nitrogen to the cationic nitrogen atoms of the NHC catalyst. The major transition structure (**Major-Michael-TS-(*S*)**) experiences greater stabilization of the anionic aoQM nitrogen via a $^{+}$NCH···N^{-} interaction[27] (Figure 4, green lines). In the minor transition structure (**Minor-Michael-TS-(*R*)**), the chiral benzyl group replaces this interaction with a significantly weaker $^{+}NCCH_2\cdots N^{-}$ interaction.[28] The computed enantioselectivity of 1.7 kcal/mol agrees well with the experimental value of 1.4 kcal/mol.

Experimental Evidence for aoQM Formation. With all computations thus far suggesting aoQM intermediacy, a model experiment was devised to test these findings. We performed the NHC **2**-catalyzed addition of benzaldehyde to *ortho*-amino benzyl chloride (Figure 5). This model reaction was chosen so that the reaction could be performed in a sufficiently large scale to provide details of the rate-determining step by measuring the ^{13}C isotope effects (IEs) at natural abundance by observing

DOI: 10.1021/acs.joc.7b00697
J. Org. Chem. 2017, 82, 7183−7189

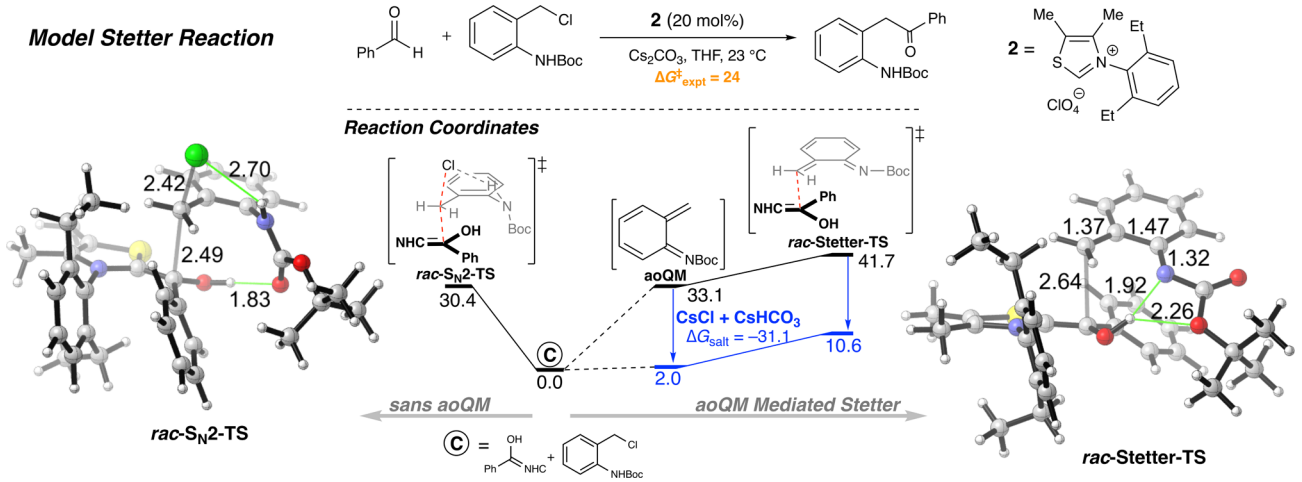

Figure 5. NHC **2**-catalyzed Stetter-type reaction of benzaldehyde. Bidirectional reaction coordinate diagrams shown. To the right, two energetics for the aoQM-mediated reaction: parent reaction without formation of any salt byproducts (black) and with Cs_2CO_3 salt byproducts (CsCl + $CsHCO_3$, blue). To the left, energetics for the non-aoQM mediated S_N2 process.

fractionation in the recovered starting materials.[29] The computed energetics were consistent with the previous reactions (Figure 5). There was a large preference for the ***rac*-Stetter-TS** (Right, blue pathway) over the ***rac*-S_N2-TS** (Left, black pathway) by ~20 kcal/mol.

In comparing the experimental and computed[30,31] isotope effects, ***rac*-S_N2-TS** and ***rac*-Stetter-TS** both showed significant KIE deviations only at C1, but the latter was in better agreement with experiments (7.3% vs 2.7% error at C1, Figure 6). Computed equilibrium isotope effects for the formation of

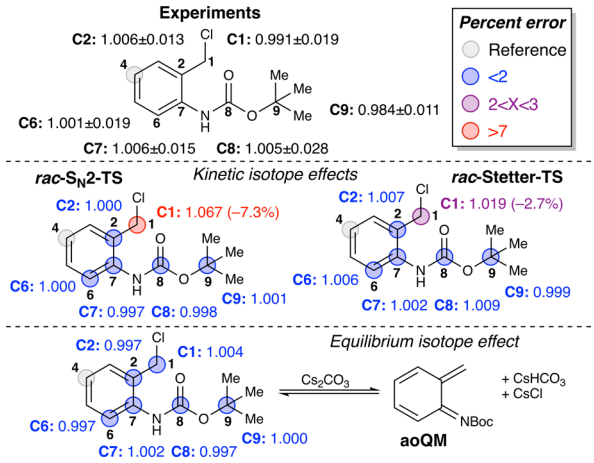

Figure 6. Natural abundance isotope effects (IE) results. Experiments (top, average of triplicate runs ± standard deviations), computed kinetic IE for S_N2 and Stetter (middle), and equilibrium IE (bottom).

the aoQM intermediate were more consistent with experimental values, and suggested this step may be rate determining. While equilibrium isotope effects are not rigorous substitutes for comparison with experimental KIE measurements, they offer a valid approximation, considering that the transition state immediately prior to aoQM formation is product-like in geometry.

Furthermore, the *N*-methylated precursor, which cannot form the aoQM, did not provide any α-aryl ketone product after 48 h, instead yielding exclusively the benzoin adduct (Scheme 2). This suggested that the preclusion of the aoQM

Scheme 2. Effect of Substrate *N*-Methylation on the NHC-Catalyzed Stetter Reaction

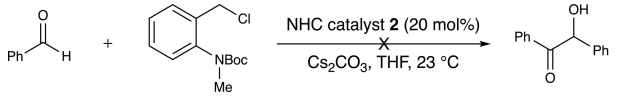

dramatically slowed down the Stetter process. We anticipated that methylation of the substrate might also affect the barrier of the nucleophilic addition step. The computed barrier of 30.3 kcal/mol (Figure 7, **Me-*rac*-S_N2-TS**) is essentially identical to

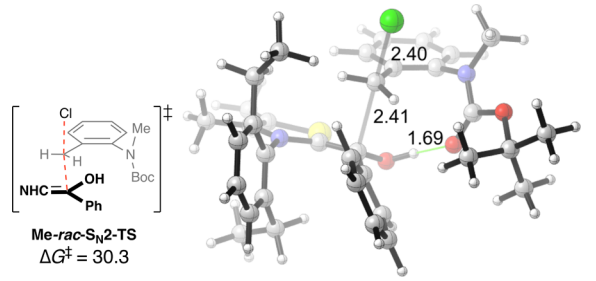

Figure 7. Computed methylated Stetter S_N2 TS showing a similar barrier to the nonmethylated parent ***rac*-S_N2-TS**.

***rac*-S_N2-TS** ($\Delta G^{\ddagger}$ = 30.4 kcal/mol), indicating that methylation likely shuts down **Deprotonation-TS** (Figures 1 and 2) without targeting the S_N2 pathway.

Analysis of the formation of imidazole-HCl indicated that while exergonic, the ~8 kcal/mol stabilization provided was not enough to drive aoQM formation (Chart 1). As an experimental test, the model Stetter reaction (Figure 5) was run with imidazole as base in place of Cs_2CO_3. As predicted by theory, there was no reaction with imidazole base (Scheme 3).

Scheme 3. Effect of Imidazole Base on the NHC-Catalyzed Stetter Reaction

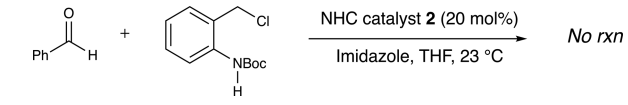

DOI: 10.1021/acs.joc.7b00697
J. Org. Chem. 2017, 82, 7183–7189

These computations and experiments, in combination with the isotope effect data, provided evidence supporting aoQM intermediacy for low temperature aoQM mediated processes (Figures 3 and 4).

CONCLUSIONS

To summarize, we have combined theory and experiments toward the understanding of the synthetic accessibility of aza-*ortho*-quinone methides, an underutilized reactive synthetic intermediate with significant potential. Specifically, we have discovered what enables the formation of aoQMs as viable reaction intermediates in synthesis under room temperature conditions. The loss of aromaticity over the course of the methide formation is balanced by the exergonic formation of metal chloride and metal bicarbonate salts (>30 kcal/mol), an independent effect from salt solubility and strength of the base. This energetic trade off is distinctly different from the parent oQMs, where the relative strength of the C═O π bond is enough to render this species accessible even in the absence of this thermodynamic and kinetic Cs_2CO_3 effect. The impact of salt formation in organocatalysis, especially in rendering high energy reactive intermediates thermodynamically accessible, is currently not well understood. We illustrate a thorough and enabling understanding that allows the community to leverage the utility and unique reactivity of aoQMs in asymmetric catalysis and chemical synthesis. These discoveries will enable a broader discovery and development platform integrating mild aoQM generation and its use in catalytic reactions, as oQM has for decades.

EXPERIMENTAL SECTION

KIE Experimental Parameters. Data was collected from a total of three Stetter reactions taken to 90.0, 88.8, and 89.7% completion, respectively.[32] The unreacted benzyl chloride from the model Stetter reaction with catalyst **2** and benzaldehyde was recovered and analyzed by quantitative ^{13}C NMR spectroscopy (see Supporting Information). All samples were prepared identically as described: 60 mg of recovered starting material was dissolved in 0.5 mL of $CDCl_3$ and then filtered through a 3 mm plug of Celite directly into a 5 mm high-precision NMR tube. Each NMR tube was filled to a constant sample height of 5 cm. Spectra were acquired on a Bruker Avance III 500 MHz spectrometer using proton-decoupled pulses with 80 s delays between pulses. 65536 data points were collected, which were then zero-filled to 256k before Fourier transformation. A zeroth order baseline correction was applied to all spectra, and integrations were measured using a ± 0.5 ppm region centered on each peak. The starting benzyl chloride used in all reactions and reference measurements came from the same synthetic batch. T1 values were measured for each sample using the inversion−recovery method to ensure the absence of any paramagnetic impurities.

General Procedure for NHC-Catalyzed Addition of Benzaldehyde to Aza-oQMs. *tert*-Butyl (2-(chloromethyl)phenyl)-carbamate (1.209 g, 5 mmol), 3-(2,6-diethylphenyl)-4,5-dimethylthiazol-3-ium perchlorate **2** (0.346 g, 1.00 mmol), 2-methoxynaphthalene (NMR internal standard, 0.395 g, 2.500 mmol), and freshly dried and powdered cesium carbonate (1.955 g, 6.00 mmol) were combined in an oven-dried 250 mL round-bottom flask fitted with a magnetic stirbar under argon. The reaction flask was evacuated under reduced pressure for 15 min, then backfilled with argon 3 times. THF (50 mL) was added and the mixture was stirred for 30 s, until all soluble materials went into solution. A 100 μL aliquot was taken for NMR analysis (T_0). Benzaldehyde (0.612 mL, 6.00 mmol) was added to the flask via syringe, and the reaction vessel was sealed and stirred vigorously under static argon. 100 μL aliquots were taken periodically to monitor consumption of the starting material. When an NMR aliquot indicated high (~90%) conversion (12−16h), the entire reaction mixture was filtered through a 1 cm pad of Celite and a final aliquot of the filtrate was taken to determine the percent conversion of benzyl chloride at the end time point (T_f). The filtered reaction mixture was concentrated under reduced pressure, and the residue was applied to a 2-in. pad of silica gel. Elution with 4:1 hexanes:ethyl acetate (until all remaining starting material had been collected, ~ 200 mL, TLC monitoring) followed by concentration of the eluent provided the crude recovered starting material. The recovered benzyl chloride was further purified by elution on a 50 g SNAP biotage column, (gradient 2−15% hexanes:ethyl acetate, 14 column volumes). The pure fractions of recovered benzyl chloride were collected, concentrated, dried under reduced pressure and then analyzed by quantitative ^{13}C NMR spectroscopy (see Supporting Information for details).

ASSOCIATED CONTENT

Supporting Information

The Supporting Information is available free of charge on the ACS Publications website at DOI: 10.1021/acs.joc.7b00697.

Cartesian coordinates, energies, experimental and computational KIE data, additional figures, and characterization of new compounds (PDF)

AUTHOR INFORMATION

Corresponding Authors

* scheidt@northwestern.edu
* paulc@science.oregonstate.edu

ORCID

Ryne C. Johnston: 0000-0002-6606-9401
Karl A Scheidt: 0000-0003-4856-3569
Paul Ha-Yeon Cheong: 0000-0001-6705-2962

Notes

The authors declare no competing financial interest.

ACKNOWLEDGMENTS

P.H.-Y.C. is the Bert and Emelyn Christensen professor of OSU, and gratefully acknowledges financial support from the Stone family and the National Science Foundation (NSF, CHE-1352663). We thank Dr. Yuyang Wu (NU) for assistance with KIE experiments. K.A.S. gratefully acknowledges support from the National Institutes of Health (NIGMS R01 GM073072). D.M.W., R.C.J., and P.H.-Y.C. also acknowledge computing infrastructure in part provided by the NSF Phase-2 CCI, Center for Sustainable Materials Chemistry (NSF CHE-1102637). D.M.W. also acknowledges support from the Johnson Research Fellowship.

REFERENCES

(1) Jaworski, A. A.; Scheidt, K. A. *J. Org. Chem.* **2016**, *81*, 10145−10153.

(2) For examples of oQMs in methodology, see: (a) Song, L.; Yao, H.; Tong, R. *Org. Lett.* **2014**, *16*, 3740−3743. (b) Spence, J. T. J; George, J. H. *Org. Lett.* **2013**, *15*, 3891−3893. (c) Liao, D.; Li, H.; Lei, X. *Org. Lett.* **2012**, *14*, 18−21. (d) Angle, S. R.; Yang, W. *J. Am. Chem. Soc.* **1990**, *112*, 4524−4528. (e) Ito, Y.; Nakajo, E.; Nakatsuka, M.; Saegusa, T. *Tetrahedron Lett.* **1983**, *24*, 2881−2884.

(3) For examples of oQMs in total synthesis, see: (a) Jeffrey, C. S.; Leonard, M. D.; Glassmire, A. E.; Dodson, C. D.; Richards, L. A.; Kato, M. J.; Dyer, L. A. *J. Nat. Prod.* **2014**, *77*, 148−153. (b) Li, H.; Jiang, J.; Liu, Z.; Lin, S.; Xia, G.; Xia, X.; Ding, B.; He, L.; Lu, Y.; She, Z. *J. Nat. Prod.* **2014**, *77*, 800−806.

(4) For examples of oQMs in natural product chemistry, see: (a) Gnaim, S.; Shabat, D. *Acc. Chem. Res.* **2014**, *47*, 2970−2984. (b) El-Sepelgy, O.; Haseloff, S.; Alamsetti, S. K.; Schneider, C. *Angew.*

DOI: 10.1021/acs.joc.7b00697
J. Org. Chem. 2017, 82, 7183−7189

Chem., Int. Ed. **2014**, *53*, 7923−7927. (c) Verga, D.; Nadai, M.; Doria, F.; Percivalle, C.; Di Antonio, M.; Palumbo, M.; Richter, S. N.; Freccero, M. *J. Am. Chem. Soc.* **2010**, *132*, 14625−14637. (d) Doria, F.; Richter, S. N.; Nadai, M.; Colloredo-Mels, S.; Mella, M.; Palumbo, M.; Freccero, M. *J. Med. Chem.* **2007**, *50*, 6570−6579.

(5) For examples of low temperature oQM formation, see: (a) Lewis, R. S.; Garza, C. J.; Dang, A. T.; Pedro, T. K. A.; Chain, W. J. *Org. Lett.* **2015**, *17*, 2278−2281. (b) Bai, W.-J.; David, J. G.; Feng, Z.-G.; Weaver, M. G.; Wu, K.-L.; Pettus, T. R. R. *Acc. Chem. Res.* **2014**, *47*, 3655−3664. and references cited therein. (c) Izquierdo, J.; Orue, A.; Scheidt, K. A. *J. Am. Chem. Soc.* **2013**, *135*, 10634−10637.

(6) For an example of slow aoQM formation even with heat, acid, base, and electrophilic activation, see: Frank, K. E.; Aubé, J. *J. Org. Chem.* **2000**, *65*, 655−666.

(7) (a) Steinhagen, H.; Corey, E. J. *Angew. Chem., Int. Ed.* **1999**, *38*, 1928−1931. (b) Steinhagen, H.; Corey, E. J. *Org. Lett.* **1999**, *1*, 823−824.

(8) Lee, A.; Younai, A.; Price, C. K.; Izquierdo, J.; Mishra, R. K.; Scheidt, K. A. *J. Am. Chem. Soc.* **2014**, *136*, 10589−10592.

(9) Liao, H.-H.; Chatupheeraphat, A.; Hsiao, C.-C.; Atodiresei, I.; Rueping, M. *Angew. Chem., Int. Ed.* **2015**, *54*, 15540−15544.

(10) For a review of aoQMs in organic synthesis, see; Wojciechowski, K. *Eur. J. Org. Chem.* **2001**, *2001*, 3587−3605.

(11) This approach may avoid potential pitfalls of relying on only theory or only experiments: (a) Clemente, F. R.; Houk, K. N. *Angew. Chem., Int. Ed.* **2004**, *43*, 5766−5768. (b) Plata, R. E.; Singleton, D. A. *J. Am. Chem. Soc.* **2015**, *137*, 3811−3826. (c) Zhu, H.; Clemente, F. R.; Houk, K. N.; Meyer, M. P. *J. Am. Chem. Soc.* **2009**, *131*, 1632−1633.

(12) The cesium effect is the ability of cesium bases to promote higher reactions yields over other bases, including their sodium and potassium analogs. See: (a) Martinez-Ariza, G.; McConnell, N.; Hulme, C. *Org. Lett.* **2016**, *18*, 1864−1867. (b) Xu, H.; Muto, K.; Yamaguchi, J.; Zhao, C.; Itami, K.; Musaev, D. G. *J. Am. Chem. Soc.* **2014**, *136*, 14834−14844. (c) Salvatore, R. N.; Nagle, A. S.; Jung, K. W. *J. Org. Chem.* **2002**, *67*, 674−683. (d) Hafez, A. M.; Taggi, A. E.; Wack, H.; Esterbrook, J.; Lectka, T. *Org. Lett.* **2001**, *3*, 2049−2051. (e) Flessner, T.; Doye, S. *J. Prakt. Chem.* **1999**, *341*, 186−190. (f) Kunz, H.; Kullmann, R.; Wernig, P.; Zimmer, J. *Tetrahedron Lett.* **1992**, *33*, 1969−1972. (g) Dijkstra, G.; Kruizinga, W. H.; Kellogg, R. M. *J. Org. Chem.* **1987**, *52*, 4230−4234.

(13) Zhao, Y.; Truhlar, D. G. *Theor. Chem. Acc.* **2008**, *120*, 215−241.

(14) Hehre, W. J.; Ditchfield, R.; Pople, J. A. *J. Chem. Phys.* **1972**, *56*, 2257−2261.

(15) The equilibrium of cesium carbonate and HCl with cesium bicarbonate and cesium chloride was investigated with explicit THF solvation in the geometry optimizations (see Supporting Information, Figure S1). The equilibrium remains highly exergonic ($\Delta G = -43$ kcal/mol), and in line with the conclusions granted from Chart 1.

(16) Miertuš, S.; Scrocco, E.; Tomasi, J. *Chem. Phys.* **1981**, *55*, 117−129.

(17) Frisch, M. J.; Trucks, G. W.; Schlegel, H. B.; Scuseria, G. E.; Robb, M. A.; Cheeseman, J. R.; Scalmani, G.; Barone, V.; Mennucci, B.; Petersson, G. A.; Nakatsuji, H.; Caricato, M.; Li, X.; Hratchian, H. P.; Izmaylov, A. F.; Bloino, J.; Zheng, G.; Sonnenberg, J. L.; Hada, M.; Ehara, M.; Toyota, K.; Fukuda, R.; Hasegawa, J.; Ishida, M.; Nakajima, T.; Honda, Y.; Kitao, O.; Nakai, H.; Vreven, T.; Montgomery, J. A., Jr.; Peralta, J. E.; Ogliaro, F.; Bearpark, M.; Heyd, J. J.; Brothers, E.; Kudin, K. N.; Staroverov, V. N.; Kobayashi, R.; Normand, J.; Raghavachari, K.; Rendell, A.; Burant, J. C.; Iyengar, S. S.; Tomasi, J.; Cossi, M.; Rega, N.; Millam, J. M.; Klene, M.; Knox, J. E.; Cross, J. B.; Bakken, V.; Adamo, C.; Jaramillo, J.; Gomperts, R.; Stratmann, R. E.; Yazyev, O.; Austin, A. J.; Cammi, R.; Pomelli, C.; Ochterski, J. W.; Martin, R. L.; Morokuma, K.; Zakrzewski, V. G.; Voth, G. A.; Salvador, P.; Dannenberg, J. J.; Dapprich, S.; Daniels, A. D.; Farkas, Ö.; Foresman, J. B.; Ortiz, J. V.; Cioslowski, J.; Fox, D. J. *Gaussian 09*, Revision D.01; Gaussian, Inc.: Wallingford CT, 2009.

(18) Weigend, F.; Ahlrichs, R. *Phys. Chem. Chem. Phys.* **2005**, *7*, 3297−3305.

(19) Neese, F. *WIREs Comput. Mol. Sci.* **2012**, *2*, 73−78.

(20) Hariharan, P. C.; Pople, J. A. *Theor. Chim. Acta* **1973**, *28*, 213−222.

(21) Kerr, J. A. *Chem. Rev.* **1966**, *66*, 465−500.

(22) (a) Pauling, L.; Wheland, G. W. J. *J. Chem. Phys.* **1933**, *1*, 362−374. (b) Hess, B. A., Jr.; Schaad, L. J. *J. Am. Chem. Soc.* **1983**, *105*, 7500−7505.

(23) Estimated room temperature (23 °C) barriers were calculated based on reaction yield and time using the Eyring equation: Eyring, H. *J. Chem. Phys.* **1935**, *3*, 107−115.

(24) Baldwin, J. E. *J. Chem. Soc., Chem. Commun.* **1976**, *18*, 734−736.

(25) Sugimoto, H.; Nakamura, S.; Ohwada, T. *J. Org. Chem.* **2007**, *72*, 10088−10095.

(26) Structure images generated using the CylView molecular visualization program: Legault, C. Y. *CYLview*, version 1.0b; Université Sherbrooke: Quebec, Canada, 2009; http://www.cylview.org.

(27) Walden, D. M.; Ogba, O. M.; Johnston, R. C.; Cheong, P. H.-Y. *Acc. Chem. Res.* **2016**, *49*, 1279−1291.

(28) Johnston, R. C.; Cheong, P. H.-Y. *Org. Biomol. Chem.* **2013**, *11*, 5057−5064.

(29) Singleton, D. A.; Thomas, A. A. *J. Am. Chem. Soc.* **1995**, *117*, 9357−9358.

(30) Isotope effects calculated using the Onyx program: Brueckner, A. C.; Cevallos, S. L.; Ogba, O. M.; Walden, D. M.; Meyer, M. P.; O'Leary, D. J.; Cheong, P. H.-Y. *Onyx*, version 1.0; Oregon State University: Corvallis, OR, USA, 2016.

(31) (a) Bigeleisen, J.; Mayer, M. G. *J. Chem. Phys.* **1947**, *15*, 261−267. (b) Bell, R. P. *The Tunnel Effect in Chemistry*; Chapman and Hall: New York, 1980. (c) Northrop, D. B. *J. Am. Chem. Soc.* **1999**, *121*, 3521−3524.

(32) Conversions were calculated relative to an internal standard using ^{1}H NMR spectroscopy.

DOI: 10.1021/acs.joc.7b00697
J. Org. Chem. 2017, 82, 7183−7189